Journal of Power Sources 198 (2012) 51–58

Contents lists available at SciVerse ScienceDirect

Journal of Power Sources

journal homepage: www.elsevier.com/locate/jpowsour

Chemically stable and coke resistant $Sm_{1-x}Ce_xFeO_{3-\delta}$ perovskites for low temperature solid oxide fuel cell anode applications

Syed M. Bukhari, Javier B. Giorgi*

Centre for Catalysis Research and Innovation, Department of Chemistry, University of Ottawa, 10 Marie Curie Prvt., Ottawa, Ontario, Canada K1N 6N5

ARTICLE INFO

Article history:
Received 22 June 2011
Received in revised form
22 September 2011
Accepted 23 September 2011
Available online 1 October 2011

Keywords:
Perovskite
Samarium iron oxide
Anode
Solid oxide fuel cell
Dry methane oxidation
Coke resistance

ABSTRACT

$Sm_{1-x}Ce_xFeO_{3-\delta}$ ($x = 0$–0.05) perovskite materials were investigated as anodes for low-temperature solid oxide fuel cells (LT-SOFCs) using dry hydrogen and dry methane fuels. Ce doping changes the electrical behaviour of $SmFeO_3$ from p-type to n-type and improves the reduction stability under the strong reducing atmosphere required at the anode. The resulting Ce doped materials presented good and stable performances as anodes under hydrogen and methane fuels. The $Sm_{0.95}Ce_{0.05}FeO_{3-\delta}$ anode showed the lowest charge transfer resistances in the series at 700 °C, 0.05 Ω cm^2 and 1.4 Ω cm^2 under dry hydrogen and methane, respectively. At 450 °C, the $Sm_{0.95}Ce_{0.01}FeO_{3-\delta}$ anode demonstrated performance with an open circuit potential (OCP) of 0.690 V and lowest R_{ct} of 1.5 kΩ cm^2 under dry methane fuel. More importantly no visible coking was found on the surface of these anodes after the performance under dry methane for ~23 h at all temperatures.

1. Introduction

Solid oxide fuel cells (SOFCs) technology converts chemical energy directly into electrical energy with high efficiency. Hydrogen has been explored as a fuel in SOFCs in the context of zero emission technologies [1–4]. However, SOFC technology may be used with readily available hydrocarbons (such as methane) making it an ideal bridging technology with high efficiency and low pollution. In this line, the deactivation of anodes due to coking has been pointed out as one of the main stumbling blocks [5–8]. To prevent coking on the anode while operating under hydrocarbon fuels, internal steam reforming has been suggested as a viable solution. Nonetheless, this has a detrimental effect on both the fuel efficiency and the power density of the cell, and it requires a heat recovery system for heating steam in the feed gas. A more efficient solution involves the preparation of efficient anode materials for the direct use of hydrocarbons as fuel (without internal steam reforming) to improve fuel efficiency and performance of the SOFC.

Conventional high temperature SOFCs operate with Ni/YSZ cermets as the anode material. The Ni/YSZ anode works well with hydrogen as fuel, but shows long term instability and poisoning from coke and sulphur under hydrocarbon fuels [9–11]. Additionally, the high operational temperature of YSZ-based SOFCs results in high cost for the technology. A recent direction of research has involved the use of ceria-based SOFCs, which can operate at lower temperatures because of the higher ionic conductivity of ceria [12]. Ceria and doped-ceria materials are also useful as anode components because of their mixed oxide ion and electronic conductivity under reducing conditions; an ability for continuous carbon cleaning due to oxygen storage/release; and good electrocatalytic activity for oxidation of methane [8,13,14]. However, although doped ceria has been predicted to have the ability to oxidize hydrogen and methane, a more reactive anode with higher electronic conductivity is required [5,14–16]. It is therefore highly desirable to find anode materials which should enable SOFCs to run at lower temperature, while being resistant towards coke and sulphur under hydrocarbon fuels. The achievement of this target is a milestone in the commercialization of SOFC technology towards cleaner energy production with lower cost and high efficiency.

Perovskite type oxides (ABO_3) have attracted considerable interest as alternative SOFC anodes due to: (i) mixed electronic and oxide ion conducting nature, (ii) chemical and reduction stability, (iii) catalytic performance, (iv) tuneability, i.e., multiple substitutions can be done at A-site, B-site and/or both A-site and B-site to obtain desirable properties [17–23]. Perovskite materials are suitable candidates as anodes for hydrocarbon fuels because their lattice oxygen provides a potential carbon cleaning mechanism depending on the chemical composition of the perovskite[24]. Despite such potential, most of the perovskite materials used to date require mixing of steam (internal steam reforming) with the

* Corresponding author. Tel.: +1 613 562 5800x6037; fax: +1 613 562 5170.
E-mail address: jgiorgi@uottawa.ca (J.B. Giorgi).

0378-7753/$ – see front matter © 2011 Elsevier B.V. All rights reserved.
doi:10.1016/j.jpowsour.2011.09.088

hydrocarbon fuel to prevent poisoning of the anode due to coking [25–27].

Ce substituted perovskites have been tested as anode and interesting results have been reported. However limited solubility of Ce at the A-site always made a challenge to obtain the perovskite with single phase composition [28]. Marina et al. reported that cerium doped lanthanum strontium titanates have good performance as SOFC anodes but these cerium doped anodes are not single phase perovskites. In fact these materials are combination of ceria and a perovskite phase [29]. Recently our group has reported a new series of perovskites with composition $Sm_{1-x}Ce_xFeO_{3\pm\lambda}$ (x = 0–0.05) [30]. These Ce doped perovskites are single phase with n-type electrical behaviour and their perovskite phase does not decompose under reducing conditions up to 900 °C. Their electrical conductivity values are comparable to most of the perovskite anodes under investigation, including YZT (yttrium zirconium titanate) and Y/Pr doped $BaCeO_3$ [31,32] which indicates their potentials as SOFC anodes. However, these materials are more suitable catalysts for SOFC anodes because they are resistant to coking when exposed to pure methane [33].

In this report, the new Ce doped perovskite materials with composition $Sm_{1-x}Ce_xFeO_{3\pm\lambda}$ (x = 0–0.05) have been investigated as SOFC anodes under both dry hydrogen and dry methane fuels. These materials present excellent performance under hydrogen and are resistant to coking under dry methane fuel in the temperature range of 450 °C and 700 °C.

2. Experimental

2.1. Powder synthesis

Trimetallic perovskites with formula $Sm_{1-x}Ce_xFeO_{3\pm\lambda}$ (x = 0–0.05) were prepared by a sol-gel method using citric acid as a complexing agent [30]. Chemicals used in this sol–gel method were iron nitrate [$Fe(NO_3)_3{\cdot}9H_2O$, AlfaAesar, >98%], cerium nitrate [$Ce(NO_3)_3{\cdot}6H_2O$, AlfaAesar, 99.5%], samarium nitrate ($Sm(NO_3)_3{\cdot}6H_2O$, AlfaAesar, 99.9%) and citric acid monohydrate [AlfaAesar, minimum 99.0%]. The three metal nitrates were weighed separately according to the desired stoichiometry keeping A-site and B-site metal ratio 1:1 ($Sm_{(1-x)} + Ce_x$:Fe = 1:1) and solutions were prepared by dissolving in de-ionized water. Citric acid monohydrate was weighed such that the ratio between citric acid and total metal content was 1:1. After dissolving citric acid into de-ionized water, the metal nitrate and citric acid solutions were mixed. This resulting solution was evaporated at 100 °C to form a gel and then dry amorphous citrate precursors. These amorphous citrate precursors were then manually ground and finally calcined at 850 °C for 24 h to form the perovskite phase. A single phase of the perovskite in each case was confirmed by powder X-ray diffraction and its composition was confirmed by XRF [30].

2.2. Button cell fabrication

To test the performance Ce doped perovskite anodes, electrolyte supported button cells were fabricated with a three-electrode geometry. The three-electrode geometry was adopted because it facilitates the separation of the performance of an electrode from the performance of the whole cell. Thus enables the evaluation and comparison of the performance of each perovskite material independently in the series as anodes. In a typical three electrode geometry both counter electrode (CE) and reference electrode (RE) are mounted on one side of electrolyte disc at a reasonable distance while the working electrode (WE) is mounted on the other side. However, one must take into account the alignment of counter and working electrodes while building this geometry because cross talk between electrodes can result in large errors in the measurements [34,35]. Although this geometry has been largely used by our group and others, we have recently switched to a more symmetrical configuration, as shown in Fig. 1 [36].

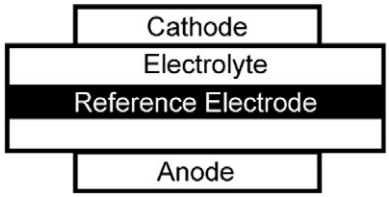

Fig. 1. Configuration of electrolyte supported button cells with three electrode geometry.

This configuration allows to: (i) minimize the cross talk between electrodes, (ii) reduce the misalignment problem of CE and WE, (iii) maximize the electrode effective area. However, the increase in thickness of the electrolyte disc results in lower measured values of the cell current and power.

In this three electrode geometry, the electrolyte is a sintered samarium doped ceria pellet of ~2 mm thickness and ~20 mm diameter, pure $Sm_{1-x}Ce_xFeO_{3\pm\lambda}$ (x = 0–0.05) perovskite materials were used as the anode, and a mixture of LSCF and SDC (50%, w/w) was used as the cathode. The reference electrode was a Pt wire wrapped around the electrolyte disc. To build the multi-electrode assembly, slurries of both anode and cathode materials were prepared in an emulsion (Triton-X100). First the anode slurry was painted and sintered at 1400 °C for 4 h. A Pt mesh together with a second coating of anode slurry was applied as the current collector and sintered again at 1400 °C for 4 h. The cathode (LSCF + SDC, 50%, w/w) slurry along with a Pt mesh was painted in the same fashion on the other side of electrolyte disc. The effective electrode area was 1.5 cm^2. The final thickness of the anode and cathode was measured as 500 and 150 μm, respectively. The reference electrode, Pt wire, was wrapped around the electrolyte disc. Pt paste was painted around the Pt wire and dried at 800 °C for 1 h. It is important to note that the contribution of Pt mesh towards performance of anodes is expected to be negligible due to the very low surface area of the Pt mesh [37].

2.3. Fuel cell setup

The detail description of the fuel cell setup used for the measurements has been already described elsewhere in the literature [36,38]. Briefly, the setup includes: 1 in. customized stainless steel ultratorr and three alumina tubes, one large diameter and other two with small diameter. The bottom part of the large diameter alumina tube is sealed into an ultratorr fitting with the help of a Viton O-ring while its top part supports the button cell. The button cell is sealed on the top of the alumina tube by a Pyrex ring. A small piece of alumina tube is placed at the top of button cell to build a pressure which facilitates a good sealing. A small diameter alumina tube is introduced from bottom of the ultratorr acting as the fuel inlet. This whole setup is suspended vertically with the help of clamps in such a way that the whole fuel cell assembly fits inside a vertically suspended tube furnace. To reduce the background electronic noise which can be introduced by the furnace, a chromel-shielded quartz tube was placed around the fuel cell and connected to ground. The tube furnace was connected to an Omron E5CN temperature controller and a K-type thermocouple was placed outside of the shielded quartz tube to measure the temperature. Sealing of the button cell on the alumina tube was done by partially melting of the Pyrex ring at 950 °C for 1 h. Three

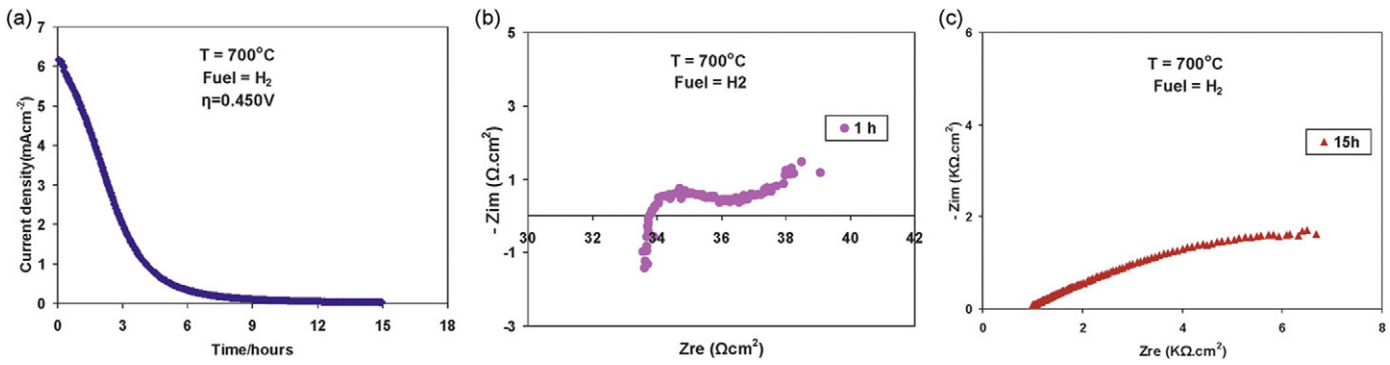

Fig. 2. Performance of undoped $SmFeO_3$ anode under dry hydrogen fuel ($x = 0$): (a) current density obtained at an overpotential of 0.450 V as a function of time. (b and c) Impedance spectra at different times during cell operation.

Pt wires were used as leads and served to connect the three electrodes, i.e., CE, WE and RE to a PARSTAT 2273 potentiostat for data collection.

2.4. Electrochemical test

The electrochemical measurements for $Sm_{1-x}Ce_xFeO_{3\pm\lambda}$ ($x = 0$–0.05) perovskite anodes were performed under two fuels: pure hydrogen and pure methane. The flow rate of fuel gas was maintained at 50 sccm with Alicat mass flow controllers. Fuel cells were operated in the temperature range of 450–700 °C and tested at temperature increments of 50 °C. A PARSTAT 2273 instrument was used to perform both AC (electrochemical impedance, EIS) and DC (chronoamperometry, CA) measurements. In all measurements a sequence of experiments was used with a total time period of ~23 h. The experiments ran in a sequence include: open circuit potential (OCP) measurement, electrochemical impedance measurement at OCP (100 kHz to 100 mHz with an AC amplitude of 10 mA), CA experiment for 15 h at an overpotential of 0.450 V, and a series of CA experiments at different overpotentials from 0 V to 1.0 V with an increment of 50 mV.

The analysis of electrochemical impedance spectra was done by using an equivalent circuit model ($L_1R_s[R_{ct}CPE_1]$) This equivalent circuit provides a serial resistance (R_s) and a charge transfer resistance (R_{ct}) for the anode which can be converted into the exchange current density (i_o) for the processes at the anode by using: $i_o = RT/nFR_{ct}$ where R is universal gas constant, T is temperature, n is number of electron involved in the charge transfer process, F is Faraday constant and R_{ct} is charge transfer resistance. The values of cell current were obtained from CA experiments which were then used to calculate cell powers.

3. Results and discussions

3.1. Performance under dry hydrogen

In trying to qualify the performance of the $Sm_{1-x}Ce_xFeO_{3\pm\lambda}$ ($x = 0$–0.05) anodes, a comparison with the undoped material is necessary. Previous work has shown that undoped $SmFeO_3$ is a semiconductor with p-type electrical behaviour [39–41] and that it decomposes when exposed to reducing gases at high temperature [30]. These properties make $SmFeO_3$ unsuitable for usage as an SOFC anode and therefore testing was limited to creating a baseline for comparison of the doped perovskites. These results also show that the contribution of the Pt current collectors to the cell performance in negligible. Fig. 2a shows the results of chronoamperometry measurements in which the cell current was measured as a function of time at an overpotential of 450 mV at 700 °C under dry hydrogen. The anode performance is observed to decrease rapidly and finally the cell current dropped to zero after ~9 h. Similarly the values of the serial and charge transfer resistances after 1 h were 33.74 Ω cm^2 and 3.25 Ω cm^2, respectively, and increased to 894 Ω cm^2 and 12580 Ω cm^2 after 15 h (Fig. 2b and c). The low performance of the undoped $SmFeO_3$ anode under dry hydrogen at the operational temperature can be linked to its very low electrical conductivity under reducing conditions due to its p-type electrical behaviour [30] and the drastic drop in performance as a function of time can be ascribed to its structure degradation [30].

To evaluate and compare the performance of Ce doped $SmFeO_3$ based anodes, the fuel cells were operated between 450 °C and 700 °C under dry hydrogen. Experimentally measured open circuit potential values for Ce doped $SmFeO_3$ anodes as a function of

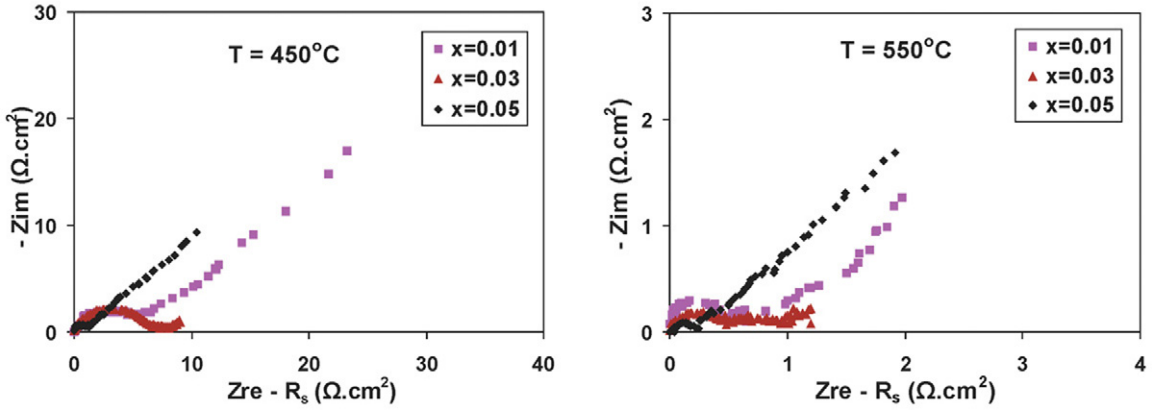

Fig. 3. Impedance spectra for $Sm_{1-x}Ce_xFeO_{3-\delta}$ ($x = 0.01$–0.05) anodes obtained at 450 °C and 550 °C in dry hydrogen fuel conditions.

Table 1
Open circuit potentials and exchange current densities (i_o) of $Sm_{1-x}Ce_xFeO_{3-\delta}$ ($x = 0.01$–0.05) anodes obtained from impedance analysis under dry hydrogen fuel.

T (°C)	$x = 0.01$		$x = 0.03$		$x = 0.05$	
	OCP (V)	i_o (mA cm^{-2})	OCP (V)	i_o (mA cm^{-2})	OCP (V)	i_o (mA cm^{-2})
450	0.977	5	0.957	8	0.986	35
500	0.973	15	0.980	25	0.974	103
550	0.956	48	0.974	82	0.960	248
600	0.927	215	0.948	248	0.924	497
700	0.863	430	0.869	595	0.844	1663

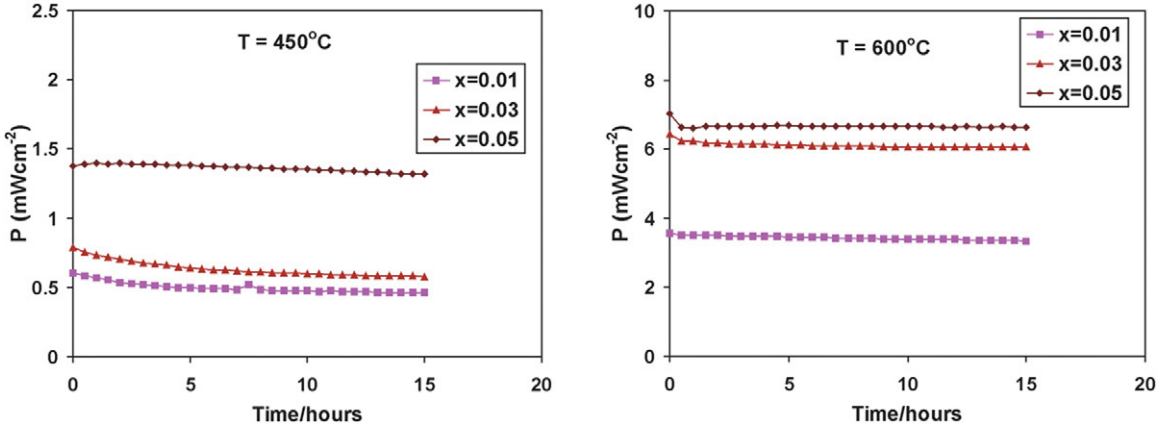

Fig. 4. Performance of $Sm_{1-x}Ce_xFeO_{3-\delta}$ ($x = 0.01$–0.05) anodes under dry hydrogen fuel. Cell powers calculated from current density obtained at an overpotential of 0.450 V as a function of time.

temperature are summarized in Table 1. The low values of OCP are typical for SOFCs utilizing an SDC electrolyte. This effect has been attributed to a partial permeability of SDC toward oxygen which permit some gas leakage across the electrolyte pellet [42], and a partial reduction of SDC near the surface of the anode under fuel conditions which causes current leakage. The OCP increases with a decrease in temperature as expected according to the Nernst's equation.

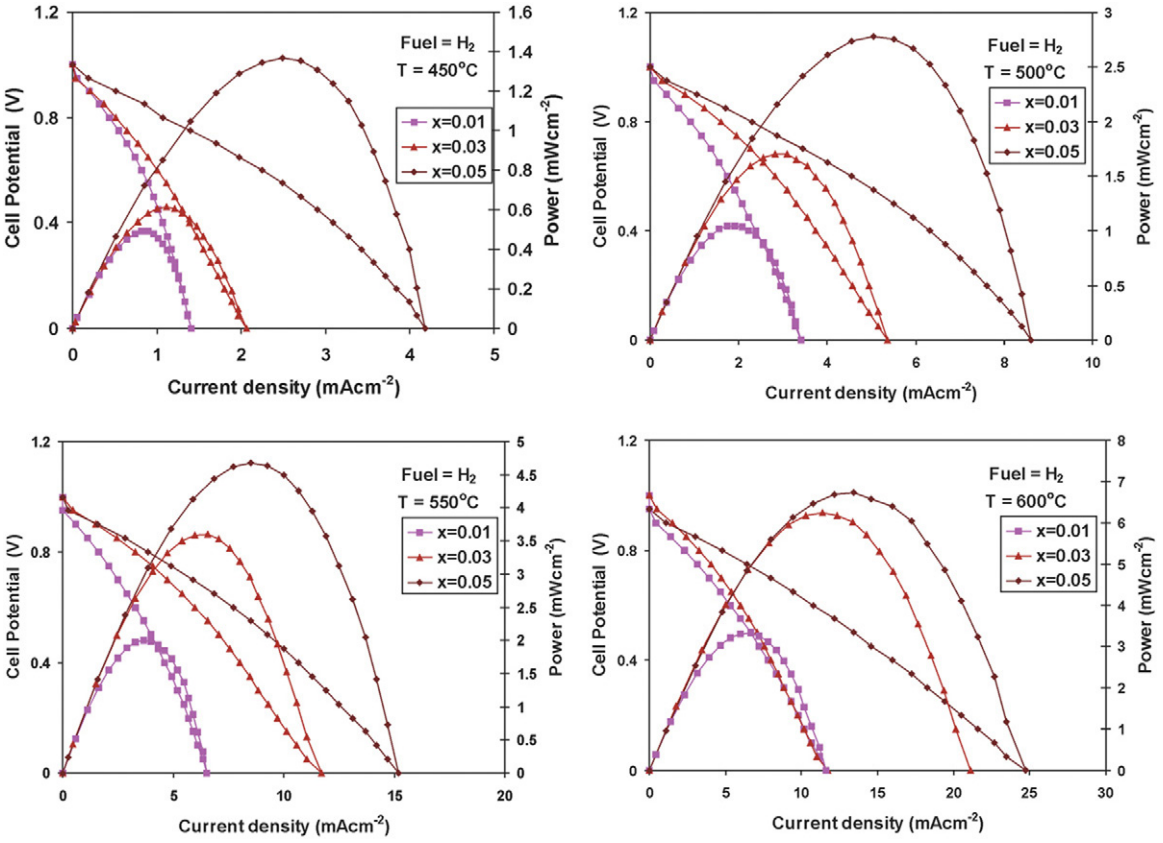

Fig. 5. *I–V* and *I–P* curves of the $Sm_xCe_{1-x}FeO_{3-\delta}$ ($x = 0.01$, 0.03 and 0.05) anodes under dry hydrogen fuel at different temperatures.

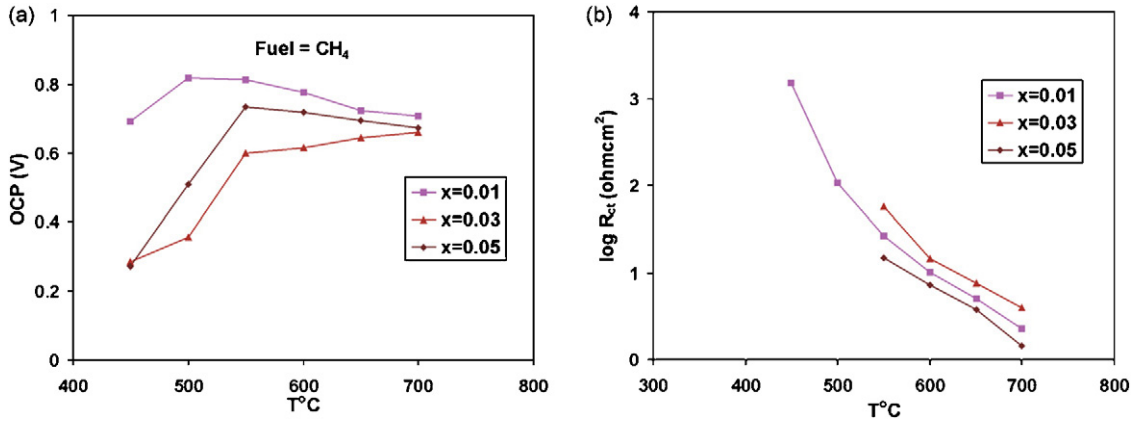

Fig. 6. (a) OCP of fuel cells. (b) Charge transfer resistances of $Sm_xCe_{1-x}FeO_{3-\delta}$ ($x = 0.01$, 0.03 and 0.05) anodes under dry methane fuel as a function of temperature.

Fig. 3 shows the impedance spectra of $Sm_{1-x}Ce_xFeO_{3-\delta}$ ($x = 0.01$–0.05) anodes at 450 °C and 550 °C under dry hydrogen as examples (at higher temperatures the arcs are smaller). The impedance plots show the characteristic semicircle for charge transfer, and a Warburg element characteristic of diffusion. The intercept of the semicircle at low frequency is the charge transfer resistance (R_{ct}) or polarization resistance (R_p). The values of charge transfer resistance were determined from fittings of an equivalent circuit model which was done by using ZSimpWin software version 3.21. The equivalent circuit considers the serial resistance of the circuit (R_s), inductance (L) due to electrical wires, inhomogeneity of the anode surface (constant phase element, Q) and a single anode polarization process which is also called as charge transfer resistance. The overall circuit can be written as $LR_s(R_{ct}Q)$. Results of the fitting showed that the charge transfer resistance decreases not only with increase in temperature but also with increase in Ce content for dry oxidation of hydrogen fuel. The activation energies calculated from Arrhenius plots revealed the same trend, i.e., the activation energy decreases with increase in Ce concentration along the series. The activation energy for $x = 0.01$, 0.03 and 0.05 are 104, 92 and 79 kJ mol^{-1}, respectively. These Ce doped $SmFeO_3$ anode materials are very good candidates for oxidation of pure hydrogen because they exhibited R_{ct} values less than 1 Ω cm^2 in the temperature range of 550–700 °C which matches well with the R_{ct} values obtained with other materials operated at higher temperature under wet hydrogen (hydrogen with 3% water contents) [1,2,4,5,27,43].

The exchange current densities calculated from charge transfer resistances for each anode are presented in Table 1. Generally, a lower charge transfer resistance (higher exchange current density) indicates a better performance of the anode. All these Ce doped $SmFeO_3$ based anodes exhibited high values of exchange current densities indicating that these materials are good candidates for SOFC anodes. Indeed, $x = 0.05$ has the best performance as anode in the series under dry hydrogen fuel. The increase in exchange current densities as a function of Ce content indicates that the introduction of Ce into the lattice of $SmFeO_3$ has actually improved its catalytic performance towards dry hydrogen oxidation.

In order to determine the reduction stability of these Ce doped $SmFeO_3$ based anodes, the cell current was measured at an overpotential of 0.450 V under dry hydrogen fuel for 15 h in each case. Fig. 4 shows the cell powers calculated from cell currents at different temperatures. The different temperature dependence of each Ce doped perovskite shows a complex behaviour that may be related to the different ratios of the redox couples Sm^{4+}/Sm^{3+} and Ce^{4+}/Ce^{3+}. In particular, the ratio Sm^{4+}/Sm^{3+} is largest for the low Ce content perovskites [30], this results in lower electronic conductivity and a reduction in power density at low temperatures. At higher temperatures, the effect is more pronounced on the lower Ce content perovskite which have the highest Sm^{4+}/Sm^{3+} ratio.

Fig. 4 shows that the values of cell powers in each case remained stable for 15 h. From this we inferred that, unlike $SmFeO_3$, these Ce doped perovskite anodes did not suffer from perovskite phase decomposition while working under the strongly reducing atmosphere of the anode chamber. This fact was further confirmed by XRD analysis of the anodes after performance, where the single perovskite phase was observed. This reduction stability of Ce doped $SmFeO_3$ perovskite materials has been described in terms of the bigger size of the Ce cation as compared to Sm [30]. In general, the bigger the size of the A-site cation in the perovskite structure, the greater the reduction stability of the perovskite.

In Fig. 5, I–V and P–I curves for $Sm_{1-x}Ce_xFeO_{3-\delta}$ ($x = 0.01$–0.05) anodes are shown at different temperatures. The P_{max} and I_{max} follow the same performance trends as shown by electrochemical impedance data. The values of both P_{max} and I_{max} have increasing trends as a function of both the temperature and Ce concentration. In the series, $x = 0.05$ has highest values of both P_{max} and I_{max}. It is important to remember that the values of P_{max} and I_{max} obtained in this work are low due to our cell design (use of very thick electrolyte) but comparison between materials is pertinent and allows selection of the best anode candidate.

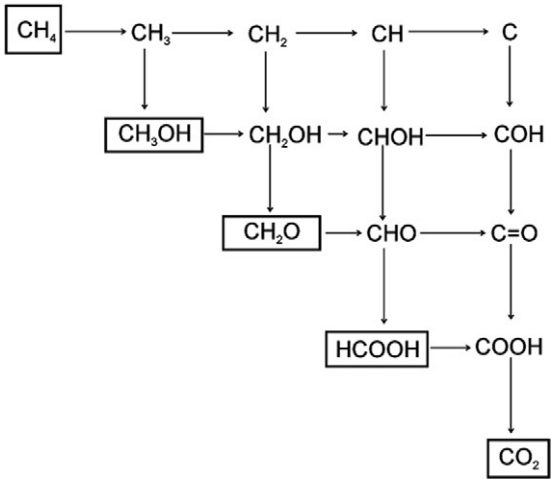

Fig. 7. Bagotzky type mechanism, showing various pathways and intermediate products that can be formed during oxidation of methane.

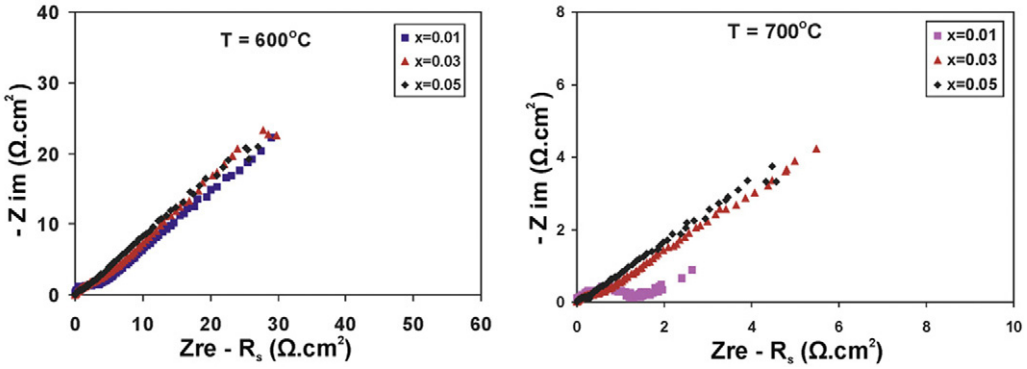

Fig. 8. Impedance spectra for $Sm_{1-x}Ce_xFeO_{3-\delta}$ ($x = 0.01$–0.05) anodes obtained at 600 °C and 700 °C under dry methane fuel conditions.

3.2. Performance under dry methane

Experimentally measured OCP values of fuel cells based on $Sm_xCe_{1-x}FeO_{3-\delta}$ ($x = 0.01$, 0.03 and 0.05) anodes under dry methane fuel are given in Fig. 6a. As expected, the OCP values are considerably lower than those measured under hydrogen due to relatively less reactive nature of methane as compared to hydrogen. Interestingly, the experimentally measured OCP values are also lower than the theoretically expected OCP values. This observation has been attributed to lower densification and internal shorting due to the mixed conductor behaviour of the SDC electrolyte in anodic conditions [42,44–46]. The observation of low OCP values at all operational temperatures as compared to theoretical Nernst's potentials suggested that it is the intrinsic property of the system and not due to the experimental setup. The open circuit potentials presented a non-linear trend as a function of both temperature and cerium content which can be attributed to multiple step oxidation of hydrocarbons (methane in this case) on the surface and establishment of an equilibrium between the hydrocarbons and partial oxidation products [47]. This also suggests different mechanisms of methane oxidation on each anode at different temperatures.

Under dry methane fuel conditions, it is expected that methane directly oxidizes on the anode consuming oxide ions (Eq. (1)).

$$CH_4 + 4O^{2-} \rightleftharpoons CO_2 + 2H_2O + 8e^- \quad (1)$$

This reaction may occur in multiple steps following a Bagotzky type mechanism (Fig. 7) where the removal of H and the addition of O to the methane may occur in a variety of mechanistic sequences [48].

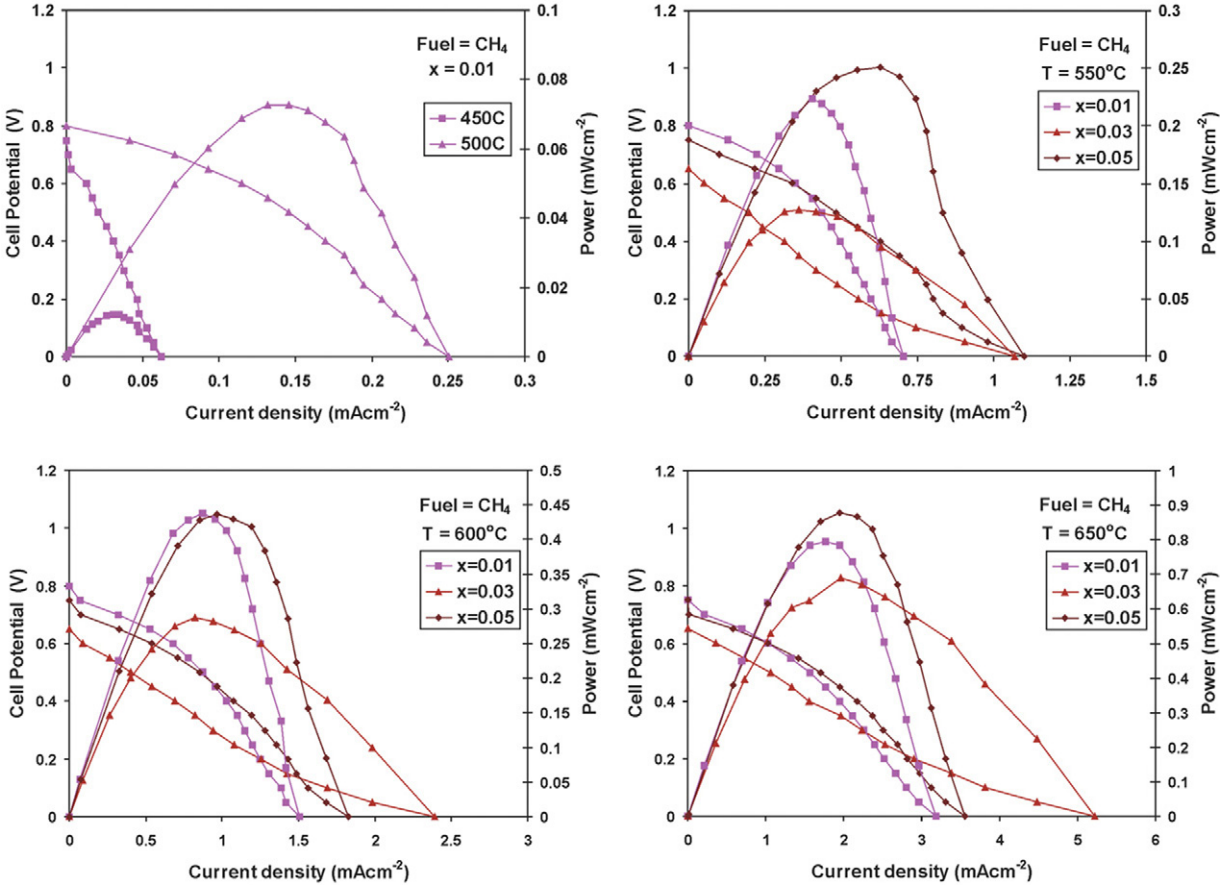

Fig. 9. *I–V* and *I–P* curves of the $Sm_xCe_{1-x}FeO_{3-\delta}$ ($x\,x = 0.01$, 0.03 and 0.05) anodes under dry methane fuel at different temperatures.

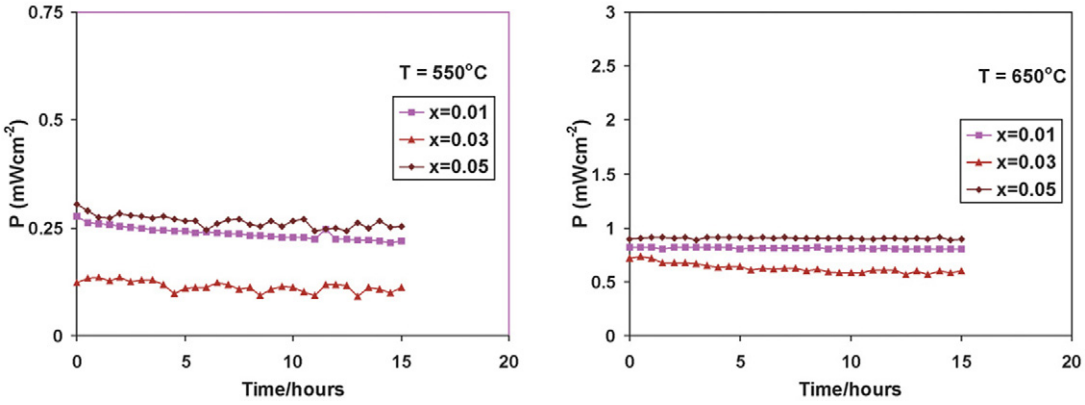

Fig. 10. Performance of $Sm_{1-x}Ce_xFeO_{3-\delta}$ ($x = 0.01–0.05$) anodes under dry methane fuel for 15 h. Cell powers calculated from current density obtained at an overpotential of 0.450 V as a function of run time.

Along the way, the mechanism may yield reactions that produce secondary (undesired) products including methanol (CH_3O), methanal (CH_2O), formic acid (HCOOH), etc. One of most likely reactions involves the partial oxidation of methane to form CO along with water (Eq. (2)). Additionally, methane can also under go thermal decomposition to form carbon and hydrogen (Eq. (3)).

$$CH_4 + 3O^{2-} \rightleftharpoons CO + 2H_2O + 6e^- \quad (2)$$

$$CH_4 \rightleftharpoons C + 2H_2 \quad (3)$$

However these by-products may be prevented from accumulating if they undergo electrochemical oxidation (Eqs. (4) and (5)).

$$C + O^{2-} \rightleftharpoons CO + 2e^- \quad (4)$$

$$CO + O^{2-} \rightleftharpoons CO_2 + 2e^- \quad (5)$$

From the above reactions, it is possible that the different OCPs that were observed are due to the contribution of each reaction in different proportions. Furthermore, the extent of contribution of each reaction depends solely on the catalytic properties of the anode materials which in turn are temperature dependent.

Electrochemical impedance plots for Ce doped $SmFeO_3$ based anodes were obtained under dry methane fuel are shown in Fig. 8 while the values of charge transfer resistance obtained after electrochemical impedance analysis of these plots are presented as a function of temperature in Fig. 6b. The values of charge transfer resistance for dry methane oxidation are higher than the charge transfer resistances of these anode materials for dry hydrogen oxidation. This can be attributed to the lower reactivity of methane as compared to hydrogen in heterogeneous oxidation [49]. Furthermore, relatively high activation values for methane oxidation revealed that these anode materials are less reactive towards methane oxidation. The activation energies calculated from the corresponding Arrhenius plots are 118 kJ mol^{-1} for $x = 0.01$, 117 kJ mol^{-1} for $x = 0.03$ and 102 kJ mol^{-1} for $x = 0.05$.

The values of charge transfer resistances have a linear trend with respect to the temperature, however, as a function of Ce contents, the trend was found to be non-linear. Indeed, the anode with 5% Ce has the lowest charge transfer resistance in the series suggesting that this anode material has the best performance as anode under dry methane fuel. The charge transfer resistance values of these anodes for dry methane oxidation (1–7 Ω cm^2 at 650–700 °C) are comparable with previously tested anodes under wet methane at higher temperatures [5,25,3,50,51]. So these Ce doped $SmFeO_3$ anode materials have the potential to oxidize methane fuel in SOFC at lower temperatures.

The relationships of cell powers and currents with cell voltage for SOFC using $Sm_xCe_{1-x}FeO_{3-\delta}$ ($x = 0.01$, 0.03 and 0.05) anodes under dry methane at different temperatures are given in Fig. 9. At lower temperatures (450 and 500 °C), only fuel cell operating with the $x = 0.01$ anode offered a reasonably high OCP. However, the values of cell power and current were low and the cells had high values of impedance resistances. At higher temperatures (550–700 °C) the cell powers and currents presented the same trend as a function of Ce contents as previously shown by charge transfer resistances. On the other hand, the cell powers and currents of the SOFC based on these Ce doped anodes gradually increases with increase in temperature.

Fig. 10 presents the performance of the fuel cells for 15 h under dry methane. The cell currents were measured against an overpotential of 0.450 V yielding the power shown. The values of cell power remained stable during the course of the test showing no significant degradation or coke poisoning. The low values of cell

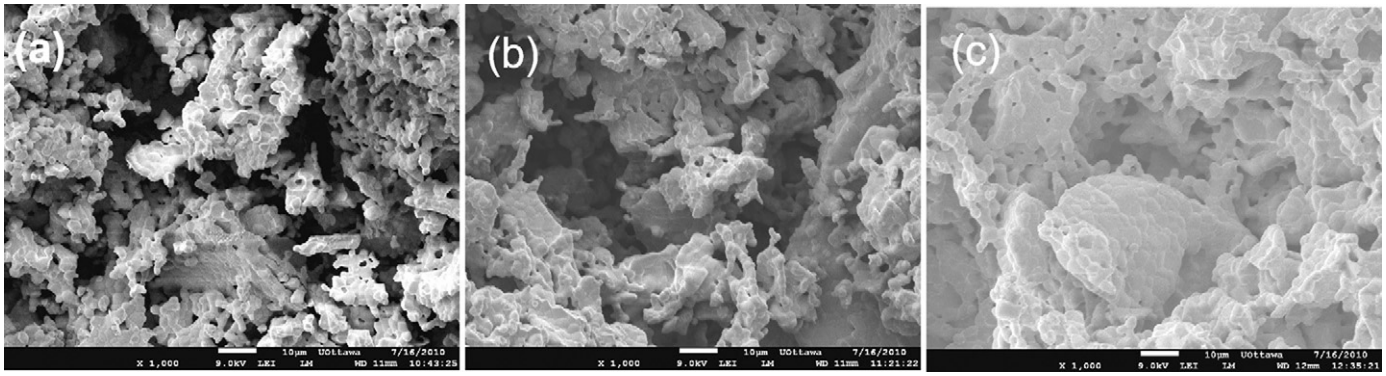

Fig. 11. SEM micrographs of $Sm_{1-x}Ce_xFeO_{3-\delta}$ anodes after performance of 23 h under dry methane. a) x = 0.01, b) x = 0.03, c) x = 0.05.

currents and powers can be ascribed to the design of the button cell (i.e., a three electrode geometry with a very thick electrolyte). Most importantly, values of cell power showed an increasing trend with temperature, while they varied non-linearly as a function of Ce contents.

XPS measurements before and after performance testing showed variations in the carbon signal within the uncertainty of the measurements and the potential formation of a small amount of amorphous carbon cannot be fully discarded. However, coke poisoning was also checked by the direct observation of the anode post-mortem (after operation under dry methane fuel for 23 h). Fig. 11 shows the SEM micrographs of used anodes. The images show that the anodes remained clear. The typical formation of carbon tubes, particles or deposits [52] was not observable. This observation strongly suggests that these materials are resistant to coke formation and will aid to developing technology for the formation of coke resistant anodes for SOFC.

4. Conclusions

Ce doped $SmFeO_3$ perovskite materials have been synthesized by a sol gel combustion method using citric acid as a complexing agent. The resulting $Sm_{1-x}Ce_xFeO_{3-\delta}$ materials were examined as anodes for SOFCs under both dry hydrogen and dry methane separately. Undoped $SmFeO_3$ material is an unviable candidate as an SOFC anode due to its p-type electrical behaviour and reduction instability under fuel atmospheres. Ce doping not only provided reduction stability but it also changed the electrical behaviour of the resulting perovskites to n-type. The new $Sm_{1-x}Ce_xFeO_{3-\delta}$ ($x = 0.01–0.05$) materials have good performance as anodes under both dry hydrogen and dry methane fuels. Indeed, the $x = 0.05$ material presented the best performance in the series under both dry hydrogen and dry methane fuels. The $x = 0.05$ anode material was able to operate under dry hydrogen at temperatures as low as 450 °C with reasonably good performance. Furthermore under dry methane fuel, $x = 0.05$ exhibited significantly lower charge transfer resistances (7–1.5 $\Omega\,cm^2$) at intermediate temperatures (600–700 °C). In light of these results, $Sm_{1-x}Ce_xFeO_{3-\delta}$, and the $x = 0.05$ anode material in particular, provide an important step forward toward reduction of fabrication costs of SOFCs by lowering their operational temperature under both dry hydrogen and dry methane fuels.

Acknowledgements

The authors are grateful for financial support provided by the Natural Sciences and Engineering Research Council of Canada (NSERC), the Ontario Research Fund, the Ontario Fuel Cell Research and Innovation Network, and the Centre for Catalysis Research and Innovation at the University of Ottawa.

References

[1] J.C. Ruiz-Morales, J. Canales-Vazquez, B. Ballesteros-Perez, J. Pena-Martinez, D. Marrero-Lopez, J.T.S. Irvine, P. Nunez, J. Eur. Ceram. Soc. 27 (2007) 4223.
[2] L. Deleebeeck, J.L. Fournier, V. Birss, Solid State Ionics 181 (2010) 1229.
[3] B.H. Smith, M.D. Gross, Electrochem. Solid-State Lett. 14 (2011) B1.
[4] A. Babaei, L. Zhang, S.L. Tan, S.P. Jiang, Solid State Ionics 181 (2010) 1221.
[5] A. Fuerte, R.X. Valenzuela, M.J. Escudero, L. Daza, J. Power Sources (2011), doi:10.1016/jpowersour.2010.12.053.
[6] B. Huang, X.F. Ye, S.R. Wang, H.W. Nie, J. Shi, Q. Hu, J.Q. Qian, X.F. Sun, T.L. Wen, J. Power Sources 162 (2006) 1172.
[7] J. Sfeir, P.A. Buffat, P. Möckli, N. Xanthopoulos, R. Vasquez, H.J. Mathieu, J.V. herle, K.R. Thampi, J. Catal. 202 (2001) 229.
[8] A. Atkinson, S. Barnett, R.J. Gorte, J.T.S. Irvine, A.J. McEvoy, M. Mogensen, S.C. Singhal, J. Vohs, Nat. Mater. 3 (2004) 17.
[9] J. Liu, V. Birss, J. Hill, AlChE J. 56 (2010) 1651.
[10] Y. Lin, Z. Zhan, J. Liu, S.A. Barnett, Solid State Ionics 176 (2005) 1827.
[11] L. Yang, Z. Cheng, M. Liu, L. Wilson, Energy Environ. Sci. 3 (2010) 1804.
[12] C. Xia, F. Chen, M. Liu, Electrochem. Solid-State Lett. 4 (2001) A52.
[13] J.B. Wang, J.-C. Jang, T.-J. Huang, J. Power Sources 122 (2003) 122.
[14] A.A. Yaremchenko, V.V. Kharton, A.A. Valente, E.V. Frolova, M.I. Ivanovskaya, A.V. Kovalevsky, F.M.B. Marques, J. Rocha, Catal. Lett. 112 (2006) 19.
[15] D. Knapp, T. Ziegler, J. Phys. Chem. C 112 (2008) 17311.
[16] N.M. Galea, D. Knapp, T. Ziegler, J. Catal. 247 (2007) 20.
[17] D.P. Fagg, V.V. Kharton, A.V. Kovalevsky, A.P. Viskup, J. Eur. Ceram. Soc. 21 (2001) 1831.
[18] A.E. Giannakas, A.A. Leontiou, A.K. Ladavos, P.J. Pomonis, Appl. Catal. A. 309 (2006) 254.
[19] T. Ishihara, H. Furutani, M. Honda, T. Yamada, T. Shibayama, T. Akbay, N. Sakai, H. Yokokawa, Y. Takita, Chem. Mater. 11 (1999) 2081.
[20] T. Ishihara, T. Yamada, H. Arikawa, H. Nishiguchi, Y. Takita, Solid State Ionics 135 (2000) 631.
[21] V.V. Kharton, A.P. Viskup, E.N. Naumovich, N.M. Lapchuk, Solid State Ionics 104 (1997) 67.
[22] C. Li, K. Chi, K. Soh, P. Wu, J. Alloys Compd. 372 (2004) 40.
[23] M.A. Pena, J.L.G. Fierro, Chem. Rev. 101 (2001) 1981.
[24] K. Urasaki, Y. Sekine, S. kawabe, E. Kikuchi, M. Matsukata, Appl. Catal. A 286 (2005) 23.
[25] E. Lay, G. Gauthier, S. Rosini, C. Savaniu, J.T.S. Irvine, Solid State Ionics 179 (2008) 1562.
[26] P. Vernoux, M. Guillodo, J. Fouletier, A. Hammou, Solid State Ionics 135 (2000) 425.
[27] S. Tao, J.T.S. Irvine, J. Electrochem. Soc. 151 (2004) A252.
[28] A. Qi, S. Wang, G. Fu, C. Ni, D. Wu, Appl. Catal. A 281 (2005) 233.
[29] O.A. Marina, L.R. Pederson, in: J. Huijsmans (Ed.), Proceeding of the 5th European Solid Oxide Fuel Cell Forum, European SOFC Forum, Switzerland, 2002, pp. 481–489.
[30] S.M. Bukhari, J.B. Giorgi, Solid State Ionics 180 (2009) 198.
[31] J.W. Fergus, Solid State Ionics 177 (2006) 1529.
[32] T. Hibino, A. Hashimoto, M. Suzuki, M. Sano, J. Electrochem. Soc. 149 (2002) A1503.
[33] S.M. Bukhari, J.B. Giorgi, ECS Trans. 28 (2010) 19.
[34] J. Winkler, P.V. Hendriksen, N. Bonanos, M. Mogensen, J. Electrochem. Soc. 145 (1998) 1184.
[35] S. McIntosh, J.M. Vohs, R.J. Gorte, J. Electrochem. Soc. 150 (2003) A1305.
[36] S.M. Bukhari, J.B. Giorgi, ECS Trans. 33 (2011) 81.
[37] C.M. Grgicak, J.B. Giorgi, J. Phys. Chem. C 111 (2007) 15446.
[38] S.M. Bukhari, J.B. Giorgi, ECS Trans. 35 (2011) 1539.
[39] Y. Itagaki, M. Mori, Y. Hosoya, H. Aono, Y. Sadaoka, Sens. Actuators B 122 (2007) 315.
[40] M.C. Carotta, G. Martinelli, Y. Sadaoka, P. Nunziante, E. Traversa, Sens. Actuators B 48 (1998) 270.
[41] Y. Hosoya, Y. Itagaki, H. Aono, Y. Sadaoka, Sens. Actuators B 108 (2005) 198.
[42] H. Shi, W. Zhou, R. Ran, Z. Shao, J. Power Sources 195 (2010) 393.
[43] N.E. Kiratzis, P. Connor, J.T.S. Irvine, J. Electroceram. 24 (2010) 270.
[44] T. Miyashita, J. Mater. Sci. 40 (2005) 6027.
[45] T. Miyashita, Open Mater. Sci. J. 3 (2009) 33.
[46] X. Zhang, M. Robertson, C. Deces-Petit, W. Qu, O. Kesler, R. Maric, D. Ghosh, J. Power Sources 164 (2007) 668.
[47] O.A. Marina, M. Mogensen, Appl. Catal. A 189 (1999) 117.
[48] V.S. Bagotzky, Y.B. Vassiliev, O.A. Khazova, J. Electroanal. Chem. 81 (1977) 229.
[49] R.J. Farrauto, M.C. Hobson, T. Kennelly, E.M. Waterman, Appl. Catal. A 81 (1992) 227.
[50] J. Qiao, N. Zhang, Z. Wang, Y. Mao, K. Sun, Y. Yuan, Fuel Cells 09 (2009) 729.
[51] D.N. Miller, J.T.S. Irvine, ECS Trans. 7 (2007) 1447.
[52] C.M. Grgicak, R.G. Green, J.B. Giorgi, J. Power Sources 179 (2008).